JACS
JOURNAL OF THE AMERICAN CHEMICAL SOCIETY

ARTICLE

pubs.acs.org/JACS

Wave Function Engineering for Ultrafast Charge Separation and Slow Charge Recombination in Type II Core/Shell Quantum Dots

Haiming Zhu, Nianhui Song, and Tianquan Lian*

Department of Chemistry, Emory University, Atlanta, Georgia 30322, United States

Supporting Information

ABSTRACT: The size dependence of optical and electronic properties of semiconductor quantum dots (QDs) have been extensively studied in various applications ranging from solar energy conversion to biological imaging. Core/shell QDs allow further tuning of these properties by controlling the spatial distributions of the conduction-band electron and valence-band hole wave functions through the choice of the core/shell materials and their size/thickness. It is possible to engineer type II core/shell QDs, such as CdTe/CdSe, in which the lowest energy conduction-band electron is largely localized in the shell while the lowest energy valence-band hole is localized in the core. This spatial distribution enables ultrafast electron transfer to the surface-adsorbed electron acceptors due to enhanced electron density on the shell materials, while simultaneously retarding the charge recombination process because the shell acts as a tunneling barrier for the core localized hole. Using ultrafast transient absorption spectroscopy, we show that in CdTe/CdSe−anthraquinone (AQ) complexes, after the initial ultrafast (∼770 fs) intra-QD electron transfer from the CdTe core to the CdSe shell, the shell-localized electron is transferred to the adsorbed AQ with a half-life of 2.7 ps. The subsequent charge recombination from the reduced acceptor, AQ^-, to the hole in the CdTe core has a half-life of 92 ns. Compared to CdSe−AQ complexes, the type II band alignment in CdTe/CdSe QDs maintains similar ultrafast charge separation while retarding the charge recombination by 100-fold. This unique ultrafast charge separation and slow recombination property, coupled with longer single and multiple exciton lifetimes in type II QDs, suggests that they are ideal light-harvesting materials for solar energy conversion.

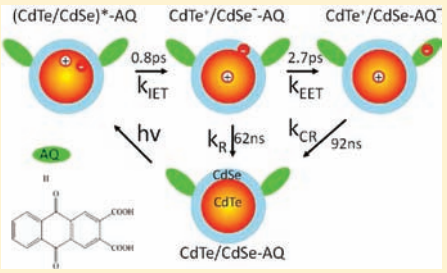

INTRODUCTION

The size-dependent optical and electronic properties of semiconductor quantum dots (QDs)[1−5] have been explored in a wide range of applications from solar energy conversion[6−10] to biological imagining.[11−14] In recent years, the effect of quantum confinement on the excited-state dynamics of QDs has also been extensively studied,[15−19] leading to the report of novel phenomena, such as long-lived hot carriers[20] and multiexciton generation (MEG).[21−24] These findings have intensified interest in QDs as light-harvesting materials because they may provide new approaches for improving the power conversion efficiency in QD-based photovoltaics.[25−29] The mechanism and efficiency of MEG has been a subject of intense recent debate, and the latest reports suggest that the MEG efficiencies in PbS and PbSe QDs are similar to those in bulk semiconductors at the same excitation wavelength.[21−24] In addition to the need to further improve MEG efficiency for practical applications, efficient utilization of multiple excitons requires their extraction prior to annihilation by Auger recombination on the 10−100 ps time scale.[15,30] With regard to the latter requirement, QDs offer a potential advantage because of the ability to dissociate excitons on the picosecond and faster time scale by interfacial charge transfer to surface-adsorbed acceptors.[27−29,31−35] Unlike in bulk semiconductors, ultrafast interfacial charge transfer in strongly quantum-confined QDs can be expected because of the larger amplitude of exciton wave function at the surface the semiconductors, enhancing electronic coupling with adsorbed acceptors. Indeed, recent proof-of-principle experiments have demonstrated that up to three[28] and four[36] excitons per CdSe QD (generated by multiple photon absorption) can be dissociated by ultrafast electron transfer (ET) to adsorbed electron acceptors. Furthermore, hot electron injection from PbSe QDs to TiO_2[29] and MEG-enhanced incident photon-to-current conversion efficiency in PbS QD-sensitized TiO_2 solar cells[27] have also been reported.

Despite these reports of hot electron transfer as well as ultrafast single and multiple exciton dissociation, the factors controlling the rate of charge transfer from and to quantum dots remain poorly understood. Furthermore, the effective utilization of excitons in QDs requires not only fast charge separation but also a long-lived interfacial charge-separated state (or slow recombination), such that the separated charge carriers can be efficiently extracted to the external circuit in photovoltaic devices or used for photocatalysis. In a recent report, we show that in CdSe/ZnS core/shell QDs adsorbed with anthraquinone (as electron acceptors), both the rates of electron transfer from the QD to the acceptor and the subsequent recombination decrease with increasing shell thickness.[37] However, because the charge-separation rate decreases much more slowly with shell thickness than does the charge-recombination rate, it is possible to increase

Received: March 26, 2011
Published: May 02, 2011

dx.doi.org/10.1021/ja202752s | J. Am. Chem. Soc. 2011, 133, 8762–8771

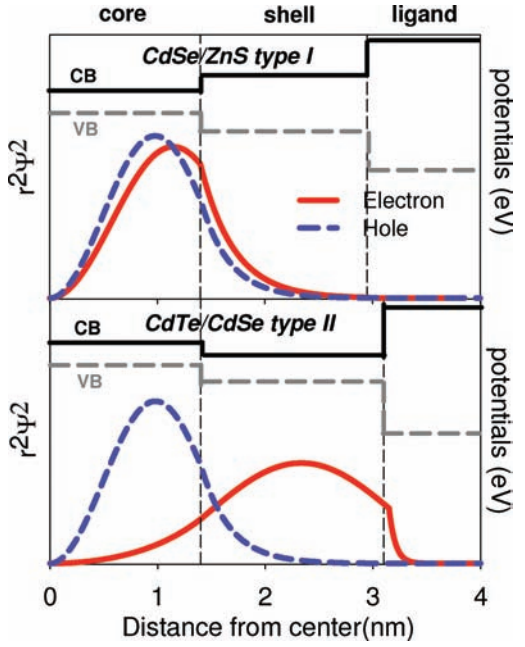

Figure 1. Radial distribution function of lowest energy (1s) conduction-band electron (solid red lines) and valence-band hole (dashed blue lines) levels of CdSe/ZnS type I (upper panel) and CdTe/CdSe type II (lower panel) core/shell QDs. Both structures have a 1.4 nm core and five monolayers of shell. Vertical dashed lines indicate core/shell and shell/ligand interfaces. Also shown are relative bulk conduction-band (CB, solid black lines) and valence-band (VB, dashed gray lines) edge positions in these materials.

the yield as well as lifetime of the charge-separated state by optimizing the shell thickness, offering an approach for engineering core/shell structures for efficient charge-transfer application. The CdSe/ZnS core/shell structure has a type I band alignment, as shown in Figure 1 (upper panel), in which both the lowest energy electrons and holes are localized in the CdSe core. The ZnS shell acts as a tunneling barrier, slowing down both the electron-transfer and recombination (or hole-transfer) processes. As a result, these type I structures would not be ideal for extracting hot carriers or multiple excitons, which require ultrafast exciton dissociation rates (to compete with hot electron relaxation and exciton−exciton annihilation, respectively).[27−29,31−35]

One possible way to simultaneously enable ultrafast charge separation and retard charge recombination is to use core−shell QDs with staggered type II band alignment, as shown in Figure 1 (lower panel), in which the lowest energy conduction-band electron and valence-band hole wave functions can be preferentially localized largely in the shell and core, respectively. It has been shown that, by selecting core/shell materials with appropriate band edge positions and tuning the degree of quantum confinement by core size and shell thickness, type II band alignment can be achieved and the spatial distributions of electron and hole wave functions can be tuned in core−shell QDs, such as CdTe/CdSe, CdSe/CdS, and CdS/ZnSe.[38−48] The spatially separated electron and hole wave functions also have beneficial effects on the absorption and excited-state dynamics of these type II QDs. In addition to the absorption bands within the core and shell materials, the charge-transfer transitions between the core and shell extend the absorption of the type II core/shell materials to longer wavelength, offering an additional approach to enhance the spectral response. The reduced electron hole overlap extends the single exciton lifetime,[45−48] reduces exciton spin relaxation rate,[49,50] and decreases Auger recombination rates. The latter leads to longer hot carrier[20] and multiexciton lifetimes,[38,51−54] enhanced optical gain,[43,55,56] and reduced blinking behavior in QDs.[57−59] All these properties suggest that type II semiconductor heterostructures should be ideal light-harvesting materials for photovoltaic and photocatalytic applications.

Scheme 1. Relevant Species Involved in Photoinduced Charge Separation and Recombination Processes in CdTe/CdSe−AQ Complexes

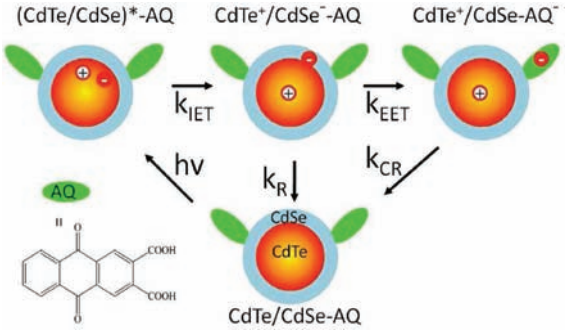

In this paper, we study the effect of type II band alignment on charge separation and recombination processes in CdTe/CdSe type II core/shell QDs adsorbed with the electron acceptor anthraquinone-2,3-dicarboxylic acid (AQ). As shown in Scheme 1, because of the type II band alignment, photoexcitation of the core/shell QD is followed by an internal charge separation, localizing the conduction-band electron in the CdSe shell (with rate constant k_{IET}) and the valence-band hole in the CdTe core, forming $CdTe^{+}/CdSe^{-}$−AQ. The 1s electron in CdSe shell can then undergo external electron transfer (with rate constant k_{EET}) to the adsorbed AQ to form the charge-separated state ($CdTe^{+}/CdSe$−AQ^{-}), competing with the electron−hole recombination process (rate constant k_R). The electron in AQ^{-} can eventually recombine with the hole in the CdTe core (with rate constant k_{CR}) to regenerate the QD and AQ ground state (CdTe/CdSe−AQ). The rates of these expected internal/external charge-separation and recombination processes were measured with transient absorption (TA) spectroscopy. As a comparison, relevant charge-separation and recombination processes in CdTe−AQ complexes are also studied. A comparison of these rates with those previously reported for CdSe−AQ and CdSe/ZnS (type I core/shell)−AQ complexes[37] shows that the unique spatial distribution of the shell-localized electron and core-localized hole in the type II core/shell QDs enables ultrafast charge separation while simultaneously retarding charge recombination.

EXPERIMENTAL DETAILS

Nanoparticle Synthesis. CdTe seed QDs were synthesized according to a previously published procedure with slight modification.[60] Briefly, 0.10 g of CdO was dissolved in a mixture of 0.45 g of 1-tetradecylphosphonic acid (TDPA) and 20 mL of 1-octadecene (ODE) by heating to about 290 °C under Ar protection. After the mixture became clear and colorless, a tellurium stock solution [0.13 g of tellurium powder dissolved in 3 mL of trioctylphosohine (TOP)] was swiftly injected. The growth of CdTe QDs was carried out at 280 °C for

dx.doi.org/10.1021/ja202752s |J. Am. Chem. Soc. 2011, 133, 8762–8771

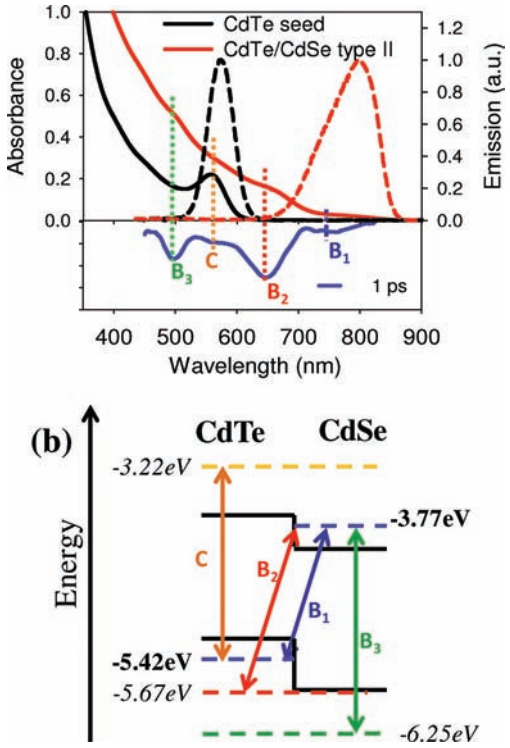

Figure 2. (a) UV−vis absorption (solid) and emission (dashed) spectra of CdTe seed (black) and corresponding CdTe/CdSe core/shell type II QDs (red). Also shown is a TA spectrum of CdTe/CdSe QDs at 1 ps delay time (see Figure 3 for details), which clearly shows four absorption bands (vertical dotted lines). (b) Energetic diagram of CdTe/CdSe type II QDs based on calculated lowest energy electron and hole levels and measured transition energies. B_1 is assigned to the lowest energy charge-transfer exciton absorption band (with a 1s hole in the CdTe core and 1s electron in the CdSe shell). B_2 and B_3 are transitions from higher valence-band levels to the 1s electron level in the CdSe shell. C is tentatively assigned to the lowest energy transition between the core localized valence-band 1s hole level to a delocalized conduction-band electron level.

10 s. After precipitation with methanol and redissolution in heptane, the size and concentration of CdTe QDs were determined for further shell coating by use of reported 1s exciton absorption band position and extinction coefficients of CdTe QDs.[61]

The growth of CdSe shells on the CdTe seed follows the previously reported successive ion layer adsorption and reaction (SILAR) method.[62] A cadmium precursor solution (0.1 M) was prepared by dissolving 0.064 g of CdO in 2.5 mL of OA (oleic acid) and 7 mL of ODE at 300 °C to obtain a colorless solution. The precursor solution was then maintained at above 100 °C. The selenium injection solution (0.1 M) was prepared by dissolving 25 mg of Se powder in 10 mL of TOP in an ultrasonic bath. The CdSe shells were grown one layer at a time, by the successive injection (2 mL/h) of calculated amounts of cadmium and selenium solutions via syringe pump. The amount of precursors required was determined by the estimated core size and shell lattice constant. It has been reported that CdTe/CdSe evolves gradually from type I to type II band alignment with increasing CdSe shell thicknesses and the transition happens at about 3 monolayers (MLs).[50,51] To confirm the formation of CdTe/CdSe type II QDs, the absorption and emission spectra of the solutions after each injection were monitored. With an estimated five layers of CdSe shell, the CdTe/CdSe QDs show pronounced absorption and emission features in the near-IR region, significantly red-shifted from the 1s exciton absorption and emission bands in the CdTe seed (see Figure 2). The actual CdTe core size and CdSe shell thickness of the CdTe/CdSe samples were determined by transmission electron microscopy (TEM). Figure S1 (Supporting Information) shows the size histograms of over 100 particles used for this study. The averaged diameter of CdTe seed is 2.86 ± 0.25 nm, agreeing reasonably well with the size estimated from the 1s exciton peak position according to an empirical formula.[61] From the measured average diameter of 6.00 ± 0.51 nm for the CdTe/CdSe QDs, the average CdSe shell thickness was determined to be 1.57 nm, which corresponds to ~4.5 MLs of wurtzite CdSe (with a lattice constant 0.35 nm/monolayer).[63]

QD (CdTe and CdTe/CdSe)−AQ complexes were prepared by the addition of AQ to QD solutions in heptane, followed by sonication and filtration to remove undissolved AQ molecules. Because AQ is insoluble in heptane, all dissolved AQ are believed to be bound to the QD surface. The ratio of the adsorbed AQ to QD was controlled to be around 2−3 by varying the amount of added AQ and was determined by ultraviolet−visible (UV−vis) absorption spectroscopy. Unlike CdSe and CdTe QDs,[61] the extinction coefficients of CdTe/CdSe QDs are not known, and their concentration were estimated from the CdTe seed used in the growth process. Because of the potential loss of CdTe/CdSe QDs in the purification steps (up to 30%), the calculated AQ:QD ratio should be considered as a lower limit.

Femtosecond Transient Visible Absorption Measurements. The femtosecond (0.1 ps−1.3 ns) transient absorption (TA) spectrometer used in this study is based on a regeneratively amplified Ti:sapphire laser system (Coherent Legend, 800 nm, 150 fs, 3 mJ/pulse, and 1 kHz repetition rate) and the Helios spectrometer (Ultrafast Systems LLC). Pump pulse at 400 nm were generated by frequency-doubling of the 800 nm pulse at a β-barium borate (BBO) crystal. The energy of the 400 nm pump pulse was controlled to be ~20 nJ/pulse by a variable neutral-density filter wheel to avoid multiexciton generation in the QD samples. The pump beam diameter at the sample is ~300 μm, corresponding to an excitation density of 0.28 μJ/cm^2. A white light continuum (from 450 to 850 nm) was generated by attenuating and focusing ~10 μJ of the 800 nm pulse into a sapphire window and splitting into a probe and reference beam. The probe beam was focused with an Al parabolic reflector onto the sample (with a beam diameter of 150 μm at the sample). The reference and probe beams were focused into a fiber optics-coupled multichannel spectrometer with complementary metal−oxide−semiconductor (CMOS) sensors and detected at a frequency of 1 kHz. The intensity of the pump and probe beams were ratioed to correct for pulse-to-pulse fluctuation of the white-light continuum. The delay between the pump and probe pulses was controlled by a motorized delay stage. The pump pulses were chopped by a synchronized chopper to 500 Hz, and the change in optical density at the sample resulted from the pump pulse was calculated. For all spectroscopy measurements, the samples were kept in a 1 mm cuvette and constantly stirred by a magnetic stirrer to avoid photodegradation.

Nanosecond Transient Absorption Measurement. Nanosecond (0.5 ns−50 μs) transient absorption was performed with the EOS spectrometer (Ultrafast Systems LLC). The pump pulses at 400 nm were generated in the regeneratively amplified Ti:sapphire laser system as described above. The white light continuum pulse (380−1700 nm, 0.5 ns pulse width, 20 kHz repetition rate) was generated by focusing a Nd:YAG laser into a photonic crystal fiber. The delay time between the pump and probe pulses was controlled by a digital delay generator (CNT-90, Pendulum Instruments). The probe and reference beams were detected by the same multichannel spectrometers used in the femtosecond setup. To connect the femtosecond and nanosecond results, the amplitude of nanosecond spectra have been slightly scaled (to account for small differences in excitation power densities) such that the spectra at delay time 0.8−1.3 ns agree with those measured by the femtosecond setup.

All data presented are averages of two independent measurements. Error bars reflect the standard deviations of the fitting parameters and half lifetimes determined from these measurements.

RESULTS AND DISCUSSION

Characterization of CdTe/CdSe Type II Quantum Dots. The UV−vis absorption and emission spectra of CdTe core-only QDs (or seeds) and corresponding CdTe/CdSe core/shell type II QDs in heptane are shown in Figure 2a. The CdTe seed QD exhibits typical absorption and emission features with a distinctive first (1s) exciton peak at ∼560 nm. In the CdTe/CdSe core/shell QD, the 1s exciton absorption peak becomes much less pronounced and a new band at ∼650 nm and a broad absorption tail extending into the near-IR are formed. Furthermore, its emission peak position (∼800 nm) is significantly red-shifted from that of the CdTe core-only QD (∼580 nm). The emission spectrum of the CdTe/CdSe QD was measured at low QD concentration with negligible reabsorption effect. Therefore, the absence of emission features in the <650 nm region suggests negligible emission from the CdTe core or CdSe shell and there is a fast internal charge transfer across the core/shell interface. These absorption and emission spectral features suggest the existence of a type II band alignment in the CdTe/CdSe core/shell QD.

Typically, in type II heterostructures (core/shell QDs,[46,50,57] nanorods,[48,49,64] or tetrapods[65,66]), the absorption spectrum exhibits transitions of both constituent materials and charge-transfer (CT) bands between them, while the emission is centered at the lowest energy CT band due to radiative recombination of the spatially separated lowest energy electron−hole pairs. As shown in Figure 2a, four absorption bands, B_1, B_2, B_3, and C (centered at ∼770, 650, 500, and 560 nm, respectively), can be indentified in the absorption spectrum of CdTe/CdSe QDs. These bands are seen more clearly in the TA spectrum at the initial delay times (such as 1 ps), which shows bleaches at these bands. As will be further explained later, these bleaches can be attributed to the filling of the conduction-band electron levels associated with these transitions. The lowest energy absorption band (B_1, centered at ∼770 nm) is near the emission peak position of this type II QD and can be assigned to the charge-transfer transition from the CdTe valence-band edge ($1s_h$) to CdSe conduction-band edge ($1s_e$). The TA spectra (see below) show that B_1, B_2, and B_3 transitions have exactly the same bleach formation and decay kinetics, suggesting that these transitions share the same electron level (i.e., the $1s_e$ in the CdSe shell). The C band is tentatively assigned to the lowest energy transition between the core localized valence-band 1s hole level to a delocalized conduction-band electron level. These assignments are further supported by the TA study of exciton dynamics and the effective mass calculation to be discussed below.

To support the assignments discussed above, we calculated the wave function and energy of the lowest energy conduction-band electron and valence-band hole in the CdTe seed and CdTe/CdSe type II QDs by treating them as particles confined in spherical wells of finite depth.[46,51,67] The effective mass of electrons (holes) is $m_e^* = 0.1$ ($m_h^* = 0.35$) in CdTe[68,69] and 0.13 (0.45) in CdSe.[63,70] The bulk conduction and valence-band edge positions are −3.67 and −5.17 V (relative to vacuum) in the CdTe core, −4.04 and −5.74 V in the CdSe shell, and 0 and −8.4 V in the surrounding organic medium.[71,72] The Coulomb interaction between the electron and hole is treated as a first-order perturbation to the energy of the 1s exciton state in the CdTe core-only QD (the dielectric constant is $\varepsilon = 10\varepsilon_0$ in CdTe).[68] This correction was neglected in the CdTe/CdSe type II QDs because of the much smaller overlap of the electron and hole wave functions. For CdTe core-only QDs with diameter of 2.86 nm, the calculated 1s exciton peak position (550 nm) agrees well with the measured value of 560 nm, suggesting the validity of the effective mass calculation for these materials.[46,50,51,67]

The calculation shows that the lowest energy electron ($1s_e$) and hole ($1s_h$) levels are largely localized in the CdSe conduction band and CdTe valence band, respectively, as shown in Figure 2b, confirming the type II band alignment in the CdTe/CdSe QD. From the calculated $1s_e$ and $1s_h$ levels (at −3.77 V and −5.42 V, respectively), the B_1 band center is estimated at 1.65 V, agreeing well the measured value of ∼1.61 V and confirming the assignment of this transition. The energies of the valence-band levels associated with transitions B_2 and B_3 are estimated to be −5.67 and −6.25 V, respectively. From the calculated $1s_h$ level position and the measured band center, the conduction level involved in transition C is estimated to be at −3.22 V. Considering the HOMO (more negative than −6.61 V) and LUMO (−4 V) levels of AQ,[37] only electron transfer from the excited QD to AQ is energetically possible.

Exciton Dynamics in Free CdTe/CdSe Type II Quantum Dots. Transient absorption spectra of free CdTe/CdSe QDs after 400 nm excitation are shown in Figure 3a upper (0−5 ps) and lower (5 ps−1 μs) panels. These spectra were obtained with low pump power (20 nJ/pulse) to ensure that the average number of excitons per QD is much less than 1 and the effect of multiexcitons on carrier relaxation dynamics is negligible. Previous studies of CdSe core-only QDs have shown that TA signals in these materials are dominated by the bleach of the 1s exciton band, which is caused by the filling of the 1s electron level.[17,18,73] Due to the Pauli exclusion principle, the single occupancy of the 2-fold degenerate 1s electron level reduces the transition probability to this level by half, giving rise to the bleach of 1s exciton band in the TA spectrum. Interestingly, there is a lack of a similar bleach due to the presence of holes, which has been attributed to the higher degeneracy and closely spaced energy levels (due to higher hole effective mass) in the valence band, as well as dark exciton states (caused by electron−hole exchange interaction).[17,18,33,74] In addition to state filling, a photoexcited electron-hole pair can generate a local electrical field, which shifts the exciton transition by Stark effect and lead to derivativelike features in the TA spectra.[75−78] This feature is not observed in free CdTe/CdSe core/shell QDs. Therefore, the formation and decay of bleach signals can be attributed to the dynamics of electrons in the corresponding conduction-band levels in the CdTe/CdSe QD.

In the first 5 ps (Figure 3a upper panel), the spectra show four separate bleaching bands centered at 560, 500, 650, and 770 nm, assigned to C, B_3, B_2, and B_1 transitions, respectively. The bleach of C band forms with a time constant of ∼300 fs (see below) and decays within ∼4 ps. Its decay leads to the growth of the bleach signals of B_1, B_2, and B_3 transitions. This relationship is clearly shown by two isosbestic points (at 532 and 599 nm) in Figure 3a (upper panel), as well as in the kinetics shown in Figure 3b. The formation of bleach features at B_1, B_2, and B_3 transitions indicates the arrival of electrons in the $1s_e$ level in the CdSe conduction band. This spectral evolution can be attributed to the internal electron localization to the CdSe conduction band within the type II core/shell QD, as shown in Scheme 1. The bleach formation kinetics of B_2 and B_1 transitions are identical,

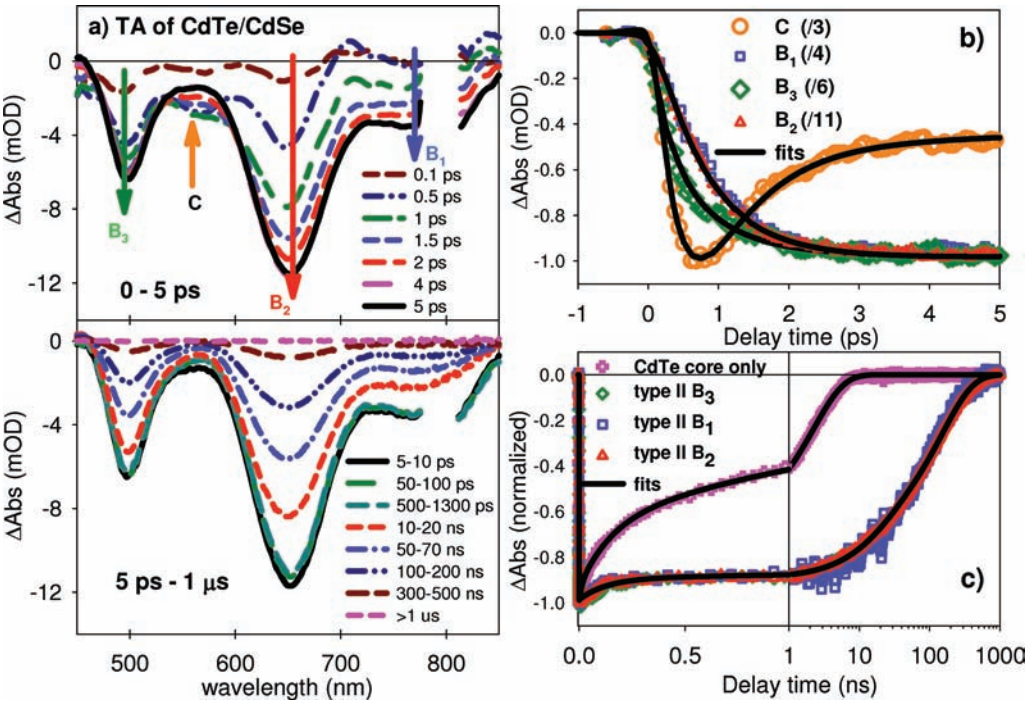

Figure 3. TA spectra and kinetics in CdTe/CdSe type II core/shell QDs. (a) Average TA spectra of free CdTe/CdSe QDs at indicated delay time windows after 400 nm excitation: upper panel, 0−5 ps; lower panel, 5 ps−1 μs. As indicated by the arrows in the upper panel, the decay of the bleach at band C leads to the growth of the bleach at B_1, B_2, and B_3 transitions. This is attributed to the internal electron transfer from the CdTe core to CdSe shell conduction band in the first 5 ps. (b) Formation and decay kinetics of the bleaches at C (560 nm), B_3 (500 nm), B_1 (770 nm), and B_2 (650 nm) bands from 0 to 5 ps. These signals have been scaled by factors indicated in the legend for better comparison. (c) Comparison of the normalized bleach recovery kinetics of B_1, B_2, and B_3 bands in the CdTe/CdSe QDs with the 1s exciton bleach recovery kinetics of the CdTe seed. The slower bleach recovery kinetics in the CdTe/CdSe QD is attributed to the longer 1s electron lifetime, consistent with type II band alignment in this material. The horizontal axis is in linear scale in the left panel (0−1 ns) and logarithmic scale in the right panel (1−1000 ns). The solid lines in panels b and c are fits to these kinetics according to eqs 1− 3 in the main text.

confirming that these transitions involve the same 1s electron level in the CdSe shell. As will be discussed below (see eq 2), the formation kinetics of B_3 is the same as B_1 and B_2 bands after its overlap with the C band is accounted for. After ~5 ps, when the internal electron localization process is completed, the TA spectra consist of bleaches of B_1, B_2, and B_3 transitions (Figure 3a, lower panel). These bleaches recover with the same kinetics (Figure 3c), reflecting the depopulation of the shell-localized 1s electron through recombination with holes in the core and/or relaxation to defect states. These electron decay kinetics were found to be the same as the QD fluorescence decay (results not shown), suggesting that the lifetime of the conduction-band electrons is controlled by the electron−hole recombination process.

The kinetics of bleach formation and decay in CdTe/CdSe QDs can be fit to obtain the rates of IET and recombination. The kinetics of C, B_1, B_2, and B_3 bleaches are fit by the following model:

$$\Delta A(B_1, B_2) = -\left[\sum_{i=3} a_i e^{-k_{Ri}t} - e^{-k_{IET}t}\right] \quad (1)$$

$$\Delta A(B_3) = \left[\sum_{i=3} a_i e^{-k_{Ri}t} - e^{-k_{IET}t}\right] - c_2\left[e^{-k_{IET}t} - e^{-k_0 t}\right] \quad (2)$$

$$\Delta A(C) = -\left[e^{-k_{IET}t} - e^{-k_0 t}\right] - c_1\left[\sum_{i=3} a_i e^{-k_{Ri}t} - e^{-k_{IET}t}\right] \quad (3)$$

Here, k_0 is the 1s exciton bleach formation rate in the CdTe core. k_{IET} is the internal electron-transfer rate from the CdTe to CdSe conduction band. a_i and k_{Ri} (i = 1−3) are the amplitudes and time constants of the multiple-exponential function that describes the decay of the 1s electron in the CdSe shell. The bleach kinetics of the C and B_3 transitions are complicated by their spectral overlap. The last term in eq 3 accounts for the contribution of B_3 transition (with amplitude c_1) at the C band. Similarly, the last term in eq 2 corrects for the contribution of transition C (amplitude c_2) at the B_3 band.

As shown in Figure 3b,c, global fitting of these kinetics by eqs 1−3 yields satisfactory fits to all kinetics traces, supporting the assignment of these transitions as well as the internal charge separation and recombination processes described above. The fitting parameters are listed in Table S1 (Supporting Information). The best fit value for the C bleach formation rate, k_0 = 3.3 ps^{-1}, reflects the relaxation of the initially excited electron to the lowest energy level in the CdTe core. This relaxation time is similar to that in CdTe (see below) and CdSe core-only QDs of similar sizes.[18,28] The best fit yields k_{IET} = 1.3 ps^{-1} (or an internal electron localization time of 0.77 ps), which is in good agreement with the k_{IET} rate in similar CdTe/CdSe type II QDs determined in a previous fluorescence upconversion measurement.[79] Similar ultrafast intra-QD charge separation dynamics have also been reported in other type II materials.[64,66,80,81] From the multiple exponential fit parameters (a_i and k_{Ri}), we calculate a half-life ($\tau_{1/2,R}$) of 62 ns for the 1s electron in the CdSe shell of the CdTe/CdSe core/shell QDs.

dx.doi.org/10.1021/ja202752s |J. Am. Chem. Soc. 2011, 133, 8762–8771

The nature of the initial excited state and the C transition is not well understood. At 400 nm excitation, the initial excited state likely involves electron and hole levels that are delocalized over the core and shell, although transitions involving the CdTe core-localized hole levels or CdSe shell-localized electron levels cannot be excluded. Direct excitation of the CdSe shell should lead to a faster (similar to k_0, ~300 fs) bleach formation of B_2 and B_1 bands because of the faster relaxation within the conduction-band levels in the shell. This is not observed in the current system. However, there may exist ultrafast (<300 fs) energy transfer between the core and shell, leading to relaxation of all excitations to the lowest energy non-charge-transfer excitonic state (giving rise to the bleach at the C band), prior to the internal charge separation process.[49] This ultrafast energy-transfer process may be too fast to be resolved in the current measurement. The electron level involved in the C transition is likely delocalized over the core and shell because the measured electron localization time (0.77 ps) is considerably slower than the electron relaxation within the conduction band of core-only CdSe QDs.[18,28] It is interesting to note that the C band is at the same energy as the lowest energy 1s exciton transition of the CdTe seed (from which the core/shell QDs were prepared), suggesting that this transition likely involves the $1s_h$ level. Despite the uncertainty of the initial excited state and assignment of C band, our data clearly show that the excited electron is localized on the CdSe shell with a time constant of 0.77 ps.

As a comparison, we have also studied the exciton decay dynamics of the CdTe core-only QDs after 400 nm excitation. The TA spectra (Figure S3, Supporting Information) show the bleach of the 1s exciton band that can be attributed to the filling of the 1s electron level. The 1s exciton bleach recovery kinetics in CdTe QDs is compared with the bleach recovery kinetics in CdTe/CdSe core/shell QDs in Figure 3c. The formation of the 1s exciton bleach in CdTe can be fit by a single-exponential function with a rate constant, k_0, of 3.3 ps^{-1}. The recovery of the exciton bleach can be well fit by a three-exponential function, from which a half-life of 0.62 ns is obtained for the 1s electron in the CdTe QD. This lifetime is 100 times shorter than that in CdTe/CdSe, consistent with the slower electron−hole recombination rate expected in the type II core/shell QDs.

Charge-Transfer Dynamics in QD−AQ Complex. TA spectra of CdTe/CdSe−AQ complex, shown in Figure 4a, were acquired under the same excitation conditions as those for free CdTe/CdSe. With low excitation power density, the average number of excitons in QDs is much less than 1 and the measured TA features can be attributed to the dynamics of single exciton states. Within the first 5 ps, the TA features are similar to those in free QDs. It shows the initial formation of bleach at C band and its subsequent decay that leads to the growth of the bleaches of B_1, B_2, and B_3 transitions. These features can be attributed to the internal electron transfer from the CdTe to CdSe conduction band with a rate constant k_{IET} that is assumed to be the same as that in free CdTe/CdSe QDs.

Unlike free CdTe/CdSe QDs, the B_1, B_2, and B_3 bleaches in CdTe/CdSe−AQ complexes recover more rapidly to form a new spectral feature. The shape of this feature remains unchanged but its amplitude decreases between 150 ps and 6 μs, as shown in Figure 4a (upper panel). This spectral feature $[A_{CS}(\lambda)]$ can be attributed to the externally charge-separated state $CdTe^+/CdSe-AQ^-$ (see Scheme 1), in which the electron in the CdSe shell has been transferred to AQ. The $A_{CS}(\lambda)$ spectrum can be qualitatively described by the sum of

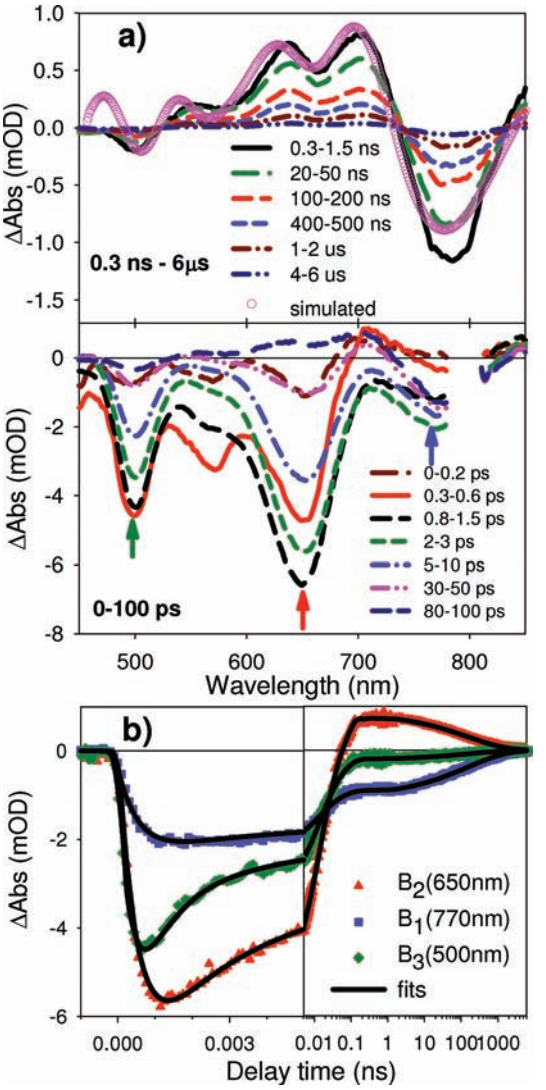

Figure 4. Transient spectra and kinetics of CdTe/CdSe−AQ complexes. (a) Average TA spectra of CdTe/CdSe−AQ at indicated delay time windows (0−100 ps, lower panel; 0.3 ns−6 μs, upper panel) after 400 nm excitation. The vertical scale in the upper panel has been expanded to show more clearly the spectra of the charge-separated state. The simulated charge-separated state spectrum (pink circles) is also shown in the upper panel. (b) Transient absorption kinetics at B_3 (500 nm), B_2 (650 nm), and B_1 (770 nm) bands (indicated by arrows in a) in CdTe/CdSe−AQ complexes. Black lines are fits according to eq 4. The delay time is in linear scale for 0−5 ps (left) and logarithmic scale for 5 ps−6 μs (right).

the spectrum of AQ^- (a broad positive absorption band around 650 nm) and a Stark-effect-induced TA spectrum of the CdTe/CdSe QD. The former was obtained in CdS/ZnS−AQ complexes, in which the photoexcitation leads to a long-lived charge separated state, $CdS^+/ZnS-AQ^-$. Because the exciton bands of CdS/ZnS QDs are below 400 nm, the TA spectra in the visible region can be attributed to the absorption of AQ^-. As shown in section S5 of the Supporting Information, the Stark-effect-induced TA feature in CdTe/CdSe QDs can be qualitatively modeled by the sum of the second-order derivative of the exciton bands, confirming its spectral assignment. Similar Stark-effect-induced TA features caused by external charge separation

dx.doi.org/10.1021/ja202752s |J. Am. Chem. Soc. 2011, 133, 8762–8771

Table 1. Half-Life Time for Charge Separation and Recombination in Complexes as Well as Conduction Band Electrons in Corresponding Free QDs. [a]

complex	$\tau_{1/2,CS}$, ps	$\tau_{1/2,CR}$, ns	$\tau_{1/2,R}$, ns
CdTe−AQ	0.85 ± 0.07	0.89 ± 0.03	0.62 ± 0.02
CdSe−AQ[37]	3.4	0.75	15
CdTe/CdSe (type II)−AQ	2.7 ± 0.3	92 ± 6	62 ± 4
CdSe/ZnS (type I)−AQ[37]	23.6	230	13

[a] Time constants for CdSe−AQ and CdSe/ZnS−AQ are taken from ref 37.

were previously observed in CdSe/ZnS−AQ complexes.[37] This spectral feature is also similar to the Stark-effect-induced spectra in CdSe quantum dots, caused by either a surface trapped charge or externally applied DC field.[75,77,82] The spatially separated electron and hole in the charge-separated state ($CdS^+/ZnS-AQ^-$) produces a local electrical field that modulates the absorption spectrum of QDs because of the different electric dipole moments and polarizabilities between the QD ground and excited states.[75,77,82] On the basis of these spectral assignments, the TA spectral evolution shown in Figure 4a indicates that, after the initial internal charge separation within the core/shell QDs, the electron in the CdSe shell is transferred to the adsorbed AQ molecule (to form AQ^-) in the first 150 ps, which is then followed by recombination of the electron in AQ^- with the hole in the CdTe core in the >150 ps time scale, as shown in Scheme 1.

The kinetics of the external charge separation and recombination can be monitored at B_1 and B_2 transitions, as shown in Figure 4b. At these wavelengths, the TA signals contain both the contributions of internally charge-separated QD excited state [$CdTe^+/CdSe^-$−AQ, with TA spectra $A_{QD^*}(\lambda)$] and the externally charge-separated state [$CdTe^+/CdSe-AQ^-$, with TA spectra $A_{CS}(\lambda)$]. The kinetics of these TA signals at the peak of B_1 and B_2 transitions can be described by the following equation:

$$\Delta A(\lambda,t) = A_{QD^*}(\lambda)\left(-e^{-k_{IET}t} + \sum_{i=3} b_i e^{-k_{EETi}t}\right) + A_{CS}(\lambda)\left(-\sum_{i=3} b_i e^{-k_{EETi}t} + e^{-(t/\tau)^{\alpha}}\right) \quad (4)$$

Here, b_i and k_{EETi} are the amplitudes and rate constants of a multiple exponential fit to the external charge separation process. τ and α are the characteristic time and exponent of the stretch exponential function used to describe the charge recombination process. k_{IET} and $A_{QD^*}(\lambda)$ have already been determined in the measurement of free CdTe/CdSe QDs under the same conditions, as shown in Figure 2. $A_{CS}(\lambda)$ is given by the TA spectra after 150 ps.

The bleach kinetics of B_2 (λ = 650 nm) and B_1 (λ = 770 nm) bands are fit according to eq 4 with b_i, k^{EETi}, τ, and α as fitting parameters. Similarly, the kinetics of the B_3 bleach (λ = 500 nm) can be described by the same model after the overlap with the C transition is accounted for, according to eq 2. As shown in Figure 4b, these kinetics are well described by the model and the fitting parameters are listed in Table S3 (Supporting Information). The best fit to the external charge separation process requires at least three exponentials, from which we calculate a

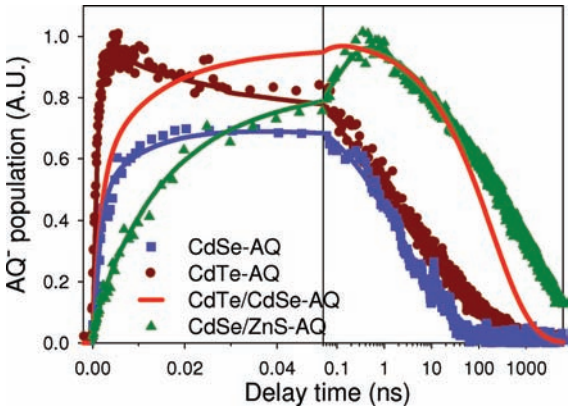

Figure 5. Comparison of AQ^- anion population kinetics in CdTe−AQ, CdTe/CdSe−AQ, CdSe−AQ, and CdSe/ZnS(2MLs)−AQ samples. The kinetics for CdTe/CdSe−AQ and CdTe−AQ complexes are extracted from eq 4 and eq S2 (Supporting Information), respectively. The AQ^- population kinetics for CdSe−AQ and CdSe/ZnS−AQ complexes have been published[37] and are replotted here. The amplitudes of these kinetics have been scaled to represent the transient quantum yields of AQ^- formation (see main text).

half-lifetime ($\tau_{1/2,CS}$) of 2.7 ps to represent the average external charge separation time. The charge recombination kinetics can be best fit by a stretched exponential function with τ = 181 ns and α = 0.42, from which a half-lifetime ($\tau_{1/2,CR}$) of 92 ns is calculated to represent the average charge recombination time.

As a comparison, the charge separation and recombination of CdTe−AQ complexes were also investigated by transient absorption spectroscopy. The details of their TA spectra, kinetics, and analysis can be found in section S3 of the Supporting Information. The half-lifetimes of charge separation ($\tau_{1/2,CS}$) and charge recombination ($\tau_{1/2,CR}$) processes are 0.85 ps and 0.89 ns, respectively. These time constants are compared with those in CdTe/CdSe QDs in Table 1. Also compared are the charge separation and recombination times previously reported for CdSe−AQ and CdSe/ZnS (2 ML)−AQ complexes.[37]

Comparison between CdSe, CdTe, CdTe/CdSe (Type II), and CdSe/ZnS (Type I) Quantum Dots. To investigate their dependence on the structures of the QDs, we compared the charge separation and recombination kinetics in core-only (CdSe and CdTe), type I core/shell (CdSe/ZnS), and type II core/shell (CdTe/CdSe) QDs. For all data shown in Figure 5, the QD:AQ ratios are similar, which enables a meaningful direct comparison of ET rates. In previous studies, we have shown that electron-transfer rates from QDs increase linearly with the number of adsorbed acceptors.[32,83,84] The kinetics of formation and decay of the charge-separated state in CdTe/CdSe−AQ complexes are obtained from the fit to the raw kinetics shown in Figure 4. Because of well-separated AQ^- and QD absorption features, the AQ^- kinetics in CdTe−AQ complexes can be obtained at ~650 nm (Figure S3, Supporting Information) and used directly for comparison. Similar kinetics of AQ^- formation and decay for CdSe−AQ and CdSe/ZnS−AQ complexes have been published previously[37] and are replotted here. The type I core/shell sample with ~2 ZnS MLs is chosen for this comparison since it is commonly used in solar cell study.[85−87] These kinetics have been scaled such that their time-dependent amplitude represents the transient quantum yield of AQ^- formation.[37] In all samples, the rates of charge separation are much faster than the intrinsic

dx.doi.org/10.1021/ja202752s |J. Am. Chem. Soc. 2011, 133, 8762–8771

electron−hole recombination time in free QDs. Therefore, all excited electrons are transferred to the adsorbates. However, due to the competition of heterogeneous charge separation and recombination processes, the transient quantum yield of the charge-separated state is time-dependent and may not reach 100% in some cases.

For CdTe/CdSe−AQ complexes, the charge-separation rate is 3 times slower than that of CdTe−AQ and is similar to that of CdSe−AQ, while the charge-recombination rate is ∼100 times slower than that of core-only (CdTe and CdSe) QDs. This comparison suggests that the type II band alignment enables ultrafast charge separation while retarding charge recombination. As shown in Figure 5, the highest yield of charge-separated state in CdSe core-only QDs is ∼70%, due to the fast charge recombination process. By maintaining the charge-separation rate and greatly slowing down the charge-recombination rate in type II QDs, a higher transient yield (∼100% at the peak) and longer lifetime of the charge-separated state can be achieved. In principle, this property of the type II QDs should allow more efficient extraction of the separated charge carriers for either electricity generation in solar cells or photocatalysis in solar-to-fuel conversion devices.

The variations of charge-separation rates in these materials can be understood within the framework of the Marcus theory of electron transfer, according to which the electron-transfer rate depends on the free energy change, electronic coupling strength, and reorganization energy.[88] Due to the delocalized electron wave functions in the QDs, the reorganization energy for the ET process is dominated by the contribution of adsorbates, and can be assumed to be the same in all these samples. The estimated 1s electron energy in CdTe/CdSe, CdTe seed, and CdSe (with first exciton peak at ∼520 nm) QDs is −3.77, −3.10, and −3.63 V (vs vacuum level), respectively. Thus, ET from CdTe/CdSe and CdSe core-only QDs to AQ have similar driving forces, and any difference in rate can be attributed to variations in the electronic coupling strength. In a previous study of type I core/shell CdSe/ZnS−AQ complexes, we showed that the electronic coupling strength for the charge separation and recombination processes is proportional to 1s electron and hole densities, respectively, at the ZnS surface.[37] These densities are taken as the modulus square of the numerically solved envelope part of the 1s electron and hole wave functions. As shown in Figure 1 (lower panel), the type II band alignment in CdTe/CdSe QDs leads to the localization of the 1s electron in the CdSe shell. The calculated electron densities at the surface for CdSe core-only and CdTe/CdSe QDs (0.115 and 0.053 nm^{-3}, respectively) are within a factor of 2 despite the 2 times larger radius of the core/shell QDs. Their similar electron densities account for the similar electronic coupling strengths and ET rates from these materials.

The rate for the charge recombination from AQ^- is determined by the energy and surface density of the hole level in the QD. The calculated surface densities and energy are 0.104, 0.173, and 1.63×10^{-4} nm^{-3} and −6.2, −5.51, and −5.42 V, respectively, for the lowest energy valence-band hole in CdSe, CdTe, and CdTe/CdSe QDs. The calculated surface hole density in the type II core/shell structure is 1000 times smaller than in core-only QDs. This large difference can be attributed to the CdTe core localized valence-band hole in CdTe/CdSe, for which the CdSe shell acts as a tunneling barrier, reducing its density at the surface. We believe that the large reduction of the surface hole density is the main reason for the much slower charge-recombination rate in the type II core/shell structures. Unfortunately, a quantitative comparison of the charge-recombination rates in various QDs is difficult because the exact nature of the hole involved in the recombination process is unknown. The transient visible spectra probe the state filling of the 1s electron level and provide no direct information on the hole level. It is possible that the valence-band hole can be trapped at some yet-to-be-characterized defect sites prior to the charge-recombination process, affecting its energy and wave function. It should be noted that the CdSe shell, which acts as a hole tunneling barrier, should reduce the surface amplitudes of the wave functions for both the valence-band and trapped holes in the CdTe core. Thus type II core/shell structures, with shell-localized electrons and core-localized holes, enable ultrafast charge separation and retard charge recombination by selectively reducing the coupling strength for recombination without decreasing the coupling strength for charge separation.

It is also interesting to compare type I and type II core/shell structures. In a previous study we showed that both the charge-separation and -recombination rates are reduced in CdSe/ZnS type I core/shell structures, because both the 1s electron and hole wave functions are localized in the core, as shown in Figure 1. However, because of the difference in shell-thickness dependence of the electron and hole wave functions (determined by their effective masses and band offsets), a judicious choice of the shell materials, such as ZnS, can lead to much faster decreases of the recombination rates than the separation rates with shell thickness. As long as the charge-separation time is shorter than the intrinsic exciton lifetimes in QDs, it is possible to increase the charge-separation yield and lifetime by using type I core/shell architecture, as shown in Figure 5. Unlike type I QDs, type II core/shell QDs can retard the charge-recombination rate without reducing the charge-separation rate. Additionally, type II QDs offer extra advantages as light-harvesting materials for charge-transfer applications because of the long single and multiple exciton lifetimes in these materials. Compared to core-only QDs and type I QDs, both the single and multiple exciton lifetimes increases in type II heterostructures because of a reduced electron−hole overlap.[38,45−48,51−54] For example, in CdTe/CdSe−AQ both the single exciton lifetime (∼62 ns) and biexciton lifetime (∼600 ps)[51] are much longer than interfacial charge-separation time (∼3 ps) to AQ, suggesting the possibility of efficient dissociation of single and multiple excitons from these materials.

Conclusions. We have investigated charge separation and recombination kinetics in core-only (CdTe−AQ) and type II core/shell (CdTe/CdSe−AQ) QD−electron acceptor complexes and compared them with the kinetics of similar processes in CdSe−AQ and type I core/shell CdSe/ZnS−AQ complexes. Optical excitation of these QDs generates long-lived single excitons, which can be dissociated by electron transfer to the adsorbed anthraquinone. In type II CdTe/CdSe QDs, the initial intra-QD charge-separation step leads to the ultrafast transfer of the conduction-band electron from the CdTe core to the CdSe shell in ∼0.77 ps with the hole remaining in the CdTe core. The half-lifetimes of external electron transfer to the adsorbed acceptor (AQ) and the subsequent recombination of the transferred electron (in AQ^-) with the valence-band hole are 2.7 ps and 92 ns, respectively. Upon comparison with CdSe−AQ or CdTe−AQ, the charge-separation rates are similar, whereas the charge recombination is retarded by 100 times in the CdTe/CdSe−AQ complexes. This differs from type I CdSe/ZnS core/shell QDs, in which the ZnS shell slows down both the

charge-separation and charge-recombination rates. The advantageous charge-separation property of type II QDs can be attributed to the shell-localized conduction-band electron and the core-localized valence-band hole, maintaining the electronic coupling strength for charge separation while reducing the coupling strength for charge recombination. This study demonstrates that type II heterostructures, with the ability to control both the compositions and dimensions of the constituent (core/shell) materials, offer an exciting opportunity to engineer the electron and hole wave function distributions to achieve ultrafast charge separation and ultraslow charge recombination. This unique ability, coupled with long single and multiple exciton lifetimes as well as extended absorption spectra (compared to constituent materials), suggests that type II heterostructures are promising light-harvesting materials for solar energy conversion.

■ ASSOCIATED CONTENT

Supporting Information. Additional text, three figures, and three tables showing particle size distribution histograms, transient absorption spectra of CdTe QDs and CdTe−AQ complexes, fitting parameters, and modeling of the Stark-effect spectrum of the charge-separated state. This material is available free of charge via the Internet at http://pubs.acs.org.

■ AUTHOR INFORMATION

Corresponding Author
tlian@emory.edu

■ ACKNOWLEDGMENT

The work was supported by the National Science Foundation (CHE-0848556) and Petroleum Research Fund (PRF 49286-ND6). The anthroquinone used in this study was a generous gift from the late Professor Thomas L. Netzel of the Georgia State University.

■ REFERENCES

(1) Alivisatos, A. P. *Science* **1996**, *271*, 933.
(2) Brus, L. E. *J. Chem. Phys.* **1983**, *79*, 5566.
(3) Brus, L. E. *J. Chem. Phys.* **1984**, *80*, 4403.
(4) Norris, D. J.; Efros, A. L.; Rosen, M.; Bawendi, M. G. *Phys. Rev. B* **1996**, *53*, 16347.
(5) Efros, A. L.; Rosen, M. *Annu. Rev. Mater. Sci.* **2000**, *30*, 475.
(6) Gur, I.; Fromer, N. A.; Geier, M. L.; Alivisatos, A. P. *Science* **2005**, *310*, 462.
(7) Huynh, W. U.; Dittmer, J. J.; Alivisatos, A. P. *Science* **2002**, *295*, 2425.
(8) Kamat, P. *J. Phys. Chem. C* **2008**, *112*, 18737.
(9) Kamat, P. V.; Tvrdy, K.; Baker, D. R.; Radich, J. G. *Chem. Rev.* **2010**, *110*, 6664.
(10) Pattantyus-Abraham, A. G.; Kramer, I. J.; Barkhouse, A. R.; Wang, X.; Konstantatos, G.; Debnath, R.; Levina, L.; Raabe, I.; Nazeeruddin, M. K.; Gratzel, M.; Sargent, E. H. *ACS Nano* **2010**, *4*, 3374.
(11) Bruchez, M., Jr.; Moronne, M.; Gin, P.; Weiss, S.; Alivisatos, A. *Science* **1998**, *281*, 2013.
(12) Chan, W. C. W.; Nie, S. M. *Science* **1998**, *281*, 2016.
(13) Kim, S.; Lim, Y. T.; Soltesz, E. G.; De Grand, A. M.; Lee, J.; Nakayama, A.; Parker, J. A.; Mihaljevic, T.; Laurence, R. G.; Dor, D. M.; Cohn, L. H.; Bawendi, M. G.; Frangioni, J. V. *Nat. Biotechnol.* **2004**, *22*, 93.
(14) Michalet, X.; Pinaud, F. F.; Bentolila, L. A.; Tsay, J. M.; Doose, S.; Li, J. J.; Sundaresan, G.; Wu, A. M.; Gambhir, S. S.; Weiss, S. *Science* **2005**, *307*, 538.
(15) Klimov, V. I.; Mikhailovsky, A. A.; McBranch, D. W.; Leatherdale, C. A.; Bawendi, M. G. *Science* **2000**, *287*, 1011.
(16) Guyot-Sionnest, P. *Struct. Bonding (Berlin, Germany)* **2005**, *118*, 59.
(17) Klimov, V. I. *J. Phys. Chem. B* **2000**, *104*, 6112.
(18) Klimov, V. I. *Annu. Rev. Phys. Chem.* **2007**, *58*, 635.
(19) Zhang, J. *J. Phys. Chem. B* **2000**, *104*, 7239.
(20) Pandey, A.; Guyot-Sionnest, P. *Science* **2008**, *322*, 929.
(21) Pijpers, J. J. H.; Ulbricht, R.; Tielrooij, K. J.; Osherov, A.; Golan, Y.; Delerue, C.; Allan, G.; Bonn, M. *Nat. Phys.* **2009**, *5*, 811.
(22) McGuire, J. A.; Sykora, M.; Joo, J.; Pietryga, J. M.; Klimov, V. I. *Nano Lett.* **2010**, *10*, 2049.
(23) Beard, M. C.; Midgett, A. G.; Hanna, M. C.; Luther, J. M.; Hughes, B. K.; Nozik, A. J. *Nano Lett.* **2010**, *10*, 3019.
(24) Nair, G.; Geyer, S. M.; Chang, L.-Y.; Bawendi, M. G. *Phys. Rev. B* **2008**, *78*, No. 125325.
(25) Nozik, A. J. *Physica E (Amsterdam, Neth.)* **2002**, *14*, 115.
(26) Nozik, A. J. *Nano Lett.* **2010**, *10*, 2735.
(27) Sambur, J. B.; Novet, T.; Parkinson, B. A. *Science* **2010**, *330*, 63.
(28) Huang, J.; Huang, Z.; Yang, Y.; Zhu, H.; Lian, T. *J. Am. Chem. Soc.* **2010**, *132*, 4858.
(29) Tisdale, W. A.; Williams, K. J.; Timp, B. A.; Norris, D. J.; Aydil, E. S.; Zhu, X.-Y. *Science* **2010**, *328*, 1543.
(30) Nozik, A. J. *Annu. Rev. Phys. Chem.* **2001**, *52*, 193.
(31) Huang, J.; Stockwell, D.; Huang, Z.; Mohler, D. L.; Lian, T. *J. Am. Chem. Soc.* **2008**, *130*, 5632.
(32) Boulesbaa, A.; Issac, A.; Stockwell, D.; Huang, Z.; Huang, J.; Guo, J.; Lian, T. *J. Am. Chem. Soc.* **2007**, *129*, 15132.
(33) Sykora, M.; Petruska, M. A.; Alstrum-Acevedo, J.; Bezel, I.; Meyer, T. J.; Klimov, V. I. *J. Am. Chem. Soc.* **2006**, *128*, 9984.
(34) Burda, C.; Link, S.; Mohamed, M.; El-Sayed, M. *J. Phys. Chem. B* **2001**, *105*, 12286.
(35) Robel, I.; Kuno, M.; Kamat, P. V. *J. Am. Chem. Soc.* **2007**, *129*, 4136.
(36) Matylitsky, V. V.; Dworak, L.; Breus, V. V.; Basche, T.; Wachtveitl, J. *J. Am. Chem. Soc.* **2009**, *131*, 2424.
(37) Zhu, H.; Song, N.; Lian, T. *J. Am. Chem. Soc.* **2010**, *132*, 15038.
(38) Sitt, A.; Sala, F. D.; Menagen, G.; Banin, U. *Nano Lett.* **2009**, *9*, 3470.
(39) Ivanov, S. A.; Piryatinski, A.; Nanda, J.; Tretiak, S.; Zavadil, K. R.; Wallace, W. O.; Werder, D.; Klimov, V. I. *J. Am. Chem. Soc.* **2007**, *129*, 11708.
(40) Donega, C. d. M. *Chem. Soc. Rev.* **2011**, *40*, 1512.
(41) Reiss, P.; Protière, M.; Li, L. *Small* **2009**, *5*, 154.
(42) Chuang, C.-H.; Lo, S. S.; Scholes, G. D.; Burda, C. *J. Phys. Chem. Lett.* **2010**, *1*, 2530.
(43) García-Santamaría, F.; Chen, Y.; Vela, J.; Schaller, R. D.; Hollingsworth, J. A.; Klimov, V. I. *Nano Lett.* **2009**, *9*, 3482.
(44) Smith, A. M.; Mohs, A. M.; Nie, S. *Nat. Nanotechnol.* **2009**, *4*, 56.
(45) Lee, D. C.; Robel, I.; Pietryga, J. M.; Klimov, V. I. *J. Am. Chem. Soc.* **2010**, *132*, 9960.
(46) Kim, S.; Fisher, B.; Eisler, H. J.; Bawendi, M. *J. Am. Chem. Soc.* **2003**, *125*, 11466.
(47) Chen, C.-Y.; Cheng, C.-T.; Lai, C.-W.; Hu, Y.-H.; Chou, P.-T.; Chou, Y.-H.; Chiu, H.-T. *Small* **2005**, *1*, 1215.
(48) Kumar, S.; Jones, M.; Lo, S. S.; Scholes, G. D. *Small* **2007**, *3*, 1633.
(49) He, J.; Lo, S. S.; Kim, J.; Scholes, G. D. *Nano Lett.* **2008**, *8*, 4007.
(50) He, J.; Zhong, H.; Scholes, G. D. *Phys. Rev. Lett.* **2010**, *105*, No. 046601.
(51) Oron, D.; Kazes, M.; Banin, U. *Phys. Rev. B* **2007**, *75*, No. 035330.
(52) Gachet, D.; Avidan, A.; Pinkas, I.; Oron, D. *Nano Lett.* **2009**, *10*, 164.

(53) Osovsky, R.; Cheskis, D.; Kloper, V.; Sashchiuk, A.; Kroner, M.; Lifshitz, E. *Phys. Rev. Lett.* **2009**, *102*, No. 197401.
(54) Htoon, H.; Malko, A. V.; Bussian, D.; Vela, J.; Chen, Y.; Hollingsworth, J. A.; Klimov, V. I. *Nano Lett.* **2010**, *10*, 2401.
(55) Klimov, V. I.; Ivanov, S. A.; Nanda, J.; Achermann, M.; Bezel, I.; McGuire, J. A.; Piryatinski, A. *Nature* **2007**, *447*, 441.
(56) Nanda, J.; Ivanov, S. A.; Htoon, H.; Bezel, I.; Piryatinski, A.; Tretiak, S.; Klimov, V. I. *J. Appl. Phys.* **2006**, *99*, No. 034309.
(57) Chen, Y.; Vela, J.; Htoon, H.; Casson, J. L.; Werder, D. J.; Bussian, D. A.; Klimov, V. I.; Hollingsworth, J. A. *J. Am. Chem. Soc.* **2008**, *130*, 5026.
(58) Mahler, B.; Spinicelli, P.; Buil, S.; Quelin, X.; Hermier, J. P.; Dubertret, B. *Nat. Mater.* **2008**, *7*, 659.
(59) Spinicelli, P.; Buil, S.; Quelin, X.; Mahler, B.; Dubertret, B.; Hermier, J. P. *Phys. Rev. Lett.* **2009**, *102*, No. 136801.
(60) Peng, Z. A.; Peng, X. G. *J. Am. Chem. Soc.* **2001**, *123*, 183.
(61) Yu, W. W.; Qu, L. H.; Guo, W. Z.; Peng, X. G. *Chem. Mater.* **2003**, *15*, 2854.
(62) Li, J. J.; Wang, Y. A.; Guo, W. Z.; Keay, J. C.; Mishima, T. D.; Johnson, M. B.; Peng, X. G. *J. Am. Chem. Soc.* **2003**, *125*, 12567.
(63) Berger, L. I. *Semiconductor Materials*; CRC Press: Boca Raton, FL, 1997.
(64) Dooley, C. J.; Dimitrov, S. D.; Fiebig, T. *J. Phys. Chem. C* **2008**, *112*, 12074.
(65) Milliron, D. J.; Hughes, S. M.; Cui, Y.; Manna, L.; Li, J. B.; Wang, L. W.; Alivisatos, A. P. *Nature* **2004**, *430*, 190.
(66) Peng, P.; Milliron, D. J.; Hughes, S. M.; Johnson, J. C.; Alivisatos, A. P.; Saykally, R. J. *Nano Lett.* **2005**, *5*, 1809.
(67) Haus, J. W.; Zhou, H. S.; Honma, I.; Komiyama, H. *Phys. Rev. B* **1993**, *47*, 1359.
(68) Pellegrini, G.; Mattei, G.; Mazzoldi, P. *J. Appl. Phys.* **2005**, *97*, No. 073706.
(69) Masumoto, Y.; Sonobe, K. *Phys. Rev. B* **1997**, *56*, 9734.
(70) Peng, X. G.; Schlamp, M. C.; Kadavanich, A. V.; Alivisatos, A. P. *J. Am. Chem. Soc.* **1997**, *119*, 7019.
(71) Salomon, A.; Boecking, T.; Seitz, O.; Markus, T.; Amy, F.; Chan, C.; Zhao, W.; Cahen, D.; Kahn, A. *Adv. Mater.* **2007**, *19*, 445.
(72) Wei, S.-H.; Zunger, A. *Appl. Phys. Lett.* **1998**, *72*, 2011.
(73) Blackburn, J. L.; Selmarten, D. C.; Ellingson, R. J.; Jones, M.; Micic, O.; Nozik, A. J. *J. Phys. Chem. B* **2005**, *109*, 2625.
(74) Huang, J.; Huang, Z.; Jin, S.; Lian, T. *J. Phys. Chem. C* **2008**, *112*, 19734.
(75) Colvin, V. L.; Alivisatos, A. P. *J. Chem. Phys.* **1992**, *97*, 730.
(76) Empedocles, S. A.; Bawendi, M. G. *Science* **1997**, *278*, 2114.
(77) Norris, D. J.; Sacra, A.; Murray, C. B.; Bawendi, M. G. *Phys. Rev. Lett.* **1994**, *72*, 2612.
(78) Hewa-Kasakarage, N. N.; Kirsanova, M.; Nemchinov, A.; Schmall, N.; El-Khoury, P. Z.; Tarnovsky, A. N.; Zamkov, M. *J. Am. Chem. Soc.* **2009**, *131*, 1328.
(79) Chou, P. T.; Chen, C. Y.; Cheng, C. T.; Pu, S. C.; Wu, K. C.; Cheng, Y. M.; Lai, C. W.; Chou, Y. H.; Chiu, H. T. *ChemPhysChem* **2006**, *7*, 222.
(80) Chen, C.-Y.; Cheng, C.-T.; Yu, J.-K.; Pu, S.-C.; Cheng, Y.-M.; Chou, P.-T.; Chou, Y.-H.; Chiu, H.-T. *J. Phys. Chem. B* **2004**, *108*, 10687.
(81) Hewa-Kasakarage, N. N.; El-Khoury, P. Z.; Tarnovsky, A. N.; Kirsanova, M.; Nemitz, I.; Nemchinov, A.; Zamkov, M. *ACS Nano* **2010**, *4*, 1837.
(82) Sacra, A.; Norris, D. J.; Murray, C. B.; Bawendi, M. G. *J. Chem. Phys.* **1995**, *103*, 5236.
(83) Boulesbaa, A.; Huang, Z.; Wu, D.; Lian, T. *J. Phys. Chem. C* **2010**, *114*, 962.
(84) Song, N.; Zhu, H.; Jin, S.; Zhan, W.; Lian, T. *ACS Nano* **2011**, *5*, 613.
(85) Sambur, J. B.; Parkinson, B. A. *J. Am. Chem. Soc.* **2010**, *132*, 2130.
(86) Makhal, A.; Yan, H.; Lemmens, P.; Pal, S. K. *J. Phys. Chem. C* **2010**, *114*, 627.
(87) Dabbousi, B. O.; RodriguezViejo, J.; Mikulec, F. V.; Heine, J. R.; Mattoussi, H.; Ober, R.; Jensen, K. F.; Bawendi, M. G. *J. Phys. Chem. B* **1997**, *101*, 9463.
(88) Marcus, R.; Sutin, N. *Biochim. Biophys. Acta* **1985**, *811*, 265.